*Revised Manuscript with changes marked

Performance investigation of solar tower system using cascade supercritical carbon dioxide Brayton-steam Rankine cycle

Honglun Yang[a], Jing Li[b*], Qiliang Wang[a], Lijun Wu[a], María Reyes Rodríguez-Sanchez[c], Domingo Santana[c], Gang Pei[a*]

a. *Department of Thermal Science and Energy Engineering, University of Science and Technology of China, Hefei 230027, China*

b. *Research Center for Sustainable Energy Technologies, Energy and Environment Institute, University of Hull, Hull, HU6 7RX, UK*

c. *Energy Systems Engineering Group (ISE), Department of Thermal and Fluid Engineering, Universidad Carlos III de Madrid, Av. Universidad, 30, 28911, Leganes, Madrid, Spain*

* Corresponding author. Tel.: 0551-63607367. E-mail address: lijing83@ ustc.edu.cn, peigang@ustc.edu.cn

Abstract: A novel solar power tower system that integrates with the cascade supercritical carbon dioxide Brayton-steam Rankine cycle is proposed to tackle the challenges of a simple supercritical carbon dioxide system in solar power systems. It provides a large storage capacity and can react to the fluctuation of solar radiation by adjusting the mass flow rate of molten salts in the receiver and heat exchanger. The fundamental is illustrated and comprehensive mathematical models are built. Energy and exergy analysis in the heat collection and power conversion processes is conducted. A comparison between the novel system and simple supercritical carbon dioxide system is made at a design plant output of 10 MW. Results indicated that: (1) the cascade system has a lower receiver inlet temperature，wider temperature difference across the receiver, higher specific work of the thermal energy storage system and lower mass flow rate of the working fluids. The solar-thermal conversion efficiency of the receiver is improved significantly. The heat gain of the tower receiver of the novel system is 53.4 MWh, which is about 7.1 MWh more than that of the simple system. The electricity production of the cascade system is improved by 9.5% at design point; (2) The novel system can generate constant electricity in a wide range of solar radiation and offer flexible control strategy for heat collection and storage. It is a promising option for central solar tower technology with a high efficiency, large storage capacity and short payback period.

Keywords: Supercritical carbon dioxide; Brayton cycle; Rankine cycle; solar tower; Cascade system

Nomenclature

a	Ambient	HTF	heat transfer fluid
A	Area, m^2	MS	molten salt
D	Diameter, m	sCO_2	Supercritical carbon dioxide
F	view factor	SR	steam Rankine
Gr	Grashof number	STP	solar tower power
h	heat transfer coefficient $W/(m^2 \cdot K)$	TES	thermal energy storage
H	Height,m	**Subscripts**	
k	thermal conductivity, $W/(m \cdot K)$	abs	absorbed
N	Number	c	convection
Nu	Nusselt number	conv	convection
Pr	Prandtl numbers	cond	conduction
Q	Energy flux, W/m or W/m^2	f	reference solar flux or fluid
Re	Reynolds number	fc	forced convection

T	Temperature, ℃ or K	i	Inner
W	Work, W	in	inlet
α	Absorption	inf	real solar flux
β	volumetric thermal expansion coefficient, 1/K	m	mirror
ε	Emissivity	nc	natural convection
η	Efficiency	o	outer
λ	thermal conductivity, W/(m·K)	ou	outlet
Δx	Length, m	r	radiation
Abbreviation		sol	incident solar irradiation
CSP	Concentrated solar power		

1. Introduction

Concentrated solar power (CSP) is a dispatchable power generation technology that can employ cheap materials for thermal energy storage(TES) in comparison with the photovoltaic system [1]. Nowadays, the CSP systems can be classified into four main technic routines, namely solar tower power (STP) system, parabolic trough system, linear Fresnel system, dish system[2]. Among them, the STP system is point focusing technology, which has a higher solar concentration ratio and is easier to reach a higher heat collection temperature and higher efficiency[3]. However, it is not economically competitive when compared with the traditional fossil-fired power plants at the current stage[4]. Further investigations should be devoted to efficiency increment and cost reduction. To achieve a higher photo-electric efficiency, the next generation CSP systems tend to operate at a higher temperature [5].

With the increase of the operating temperature above 700℃, the chemical reaction between the water-steam and solid materials in the boiler is obviously intensified. Thus the traditional steam Rankine cycle cannot satisfy the improvement of the operating temperature[6]. The supercritical CO_2 (sCO_2) Brayton cycle has been proposed to achieve a higher temperature. The advantages of the supercritical CO_2 Brayton cycle can be summarized as follows: (a) CO_2 is an inert working fluid and possesses a significantly weaker chemical corrosion with power cycle components compared with water-steam, indicating that the inlet temperature of the gas turbine can be further improved[7]; (b) the thermal conversion efficiency of the sCO_2 cycle is remarkably higher than a water-steam Rankine cycle when the maximum operation temperature exceeds 450℃[8]; (c) the whole sCO_2 system operates under the supercritical status with high pressure(>7.38MPa). Thus the sizes of the turbine and heat exchangers are reduced significantly, leading to low thermal inertia of the power plants and flexible power output adjustment[9].

Based on the benefits mentioned above, sCO_2 Brayton system is regarded as an alternative of the traditional water/steam Rankine cycle. The various researches related to sCO_2 cycle are studied experimentally and theoretically. The sCO_2 Brayton cycle was firstly proposed by Sulzer in the 950s[10], and the performance characteristic of the sCO_2 system was firstly analyzed by Feher[11]. Dostal reported that the thermal efficiency could achieve 45.3% with a cost reduction in the power system by 18% compared to the steam Rankine cycle at the inlet temperature of 550℃[12]. Several sCO_2 layout configurations, including recompression[13] and intercooling[14], were also proposed to improve power cycle efficiency.

To date, with the demand for the severe peak load regulation of the coal-fired power plants and fast development of the CSP technologies, sCO_2 systems have attracted increasing attention by researchers.. Xu et al. summarized the key issues and challenges of the sCO_2 used for coal-fired power plants[15] and proposed solution strategies[16]. The CO_2 boiler pressure drop was decreased to the water-steam boiler level and the cascade flue gas utilization system was proposed to improve thermal conversion efficiency. The feasibility of the integrated sCO_2 with CSP systems was also evaluated and analyzed. He et al. developed an integrated model for the integrated STP system including the solar field, the molten salt (MS) solar receiver, the MS TES system, heat transfer fluid (HTF) and the sCO_2 Brayton cycle[17]. The thermal performance of the CSP system using sCO_2 as the HTF under non-uniform solar flux was studied and analyzed[18]. Thermodynamic analysis and cycle layout optimization of the MS STP system integrated with a sCO_2 Brayton cycle were carried out[19]. They pointed out that the maximum allowable MS temperature of 680℃was recommended for the STP system combined with sCO_2 Brayton cycle under the present conditions and the intercooling cycle could generally offer the highest efficiency. Reyes-Belmonte presented a single-stage sCO_2 cycle that integrated with recompression and a dense gas-particle suspension tower receiver. The solar tower power systems using gas-particle suspension receiver was regarded as one of the promising options to couple with the sCO_2 power cycle due to the high temperatures achieved and the stability of the particle[20]. Saboora et.al. presented a detailed analysis of a combined power block system using carbon dioxide integrated with a thermal energy storage system and solar field [21]. Recently, the tower receiver that employed sCO_2 as heat transfer fluid (HTF) directly was investigated. In this case, the tower receiver was regarded as a primary heat exchanger in CSP systems, thus directly applying the power cycle working fluid as the receiver HTF. The integration of five different direct-heated sCO_2 Brayton cycles into a solar power tower system was studied by He et.al. [22]. In addition, exergetic analysis of sCO_2 Brayton cycles integrated with direct CO_2 solar central receivers was carried out to demonstrate the effect of operation temperature and the cycle layout on the overall performance and exergy loss[23].

Desipte of the extensive investigation, there are some technical issues and challenges of combining the sCO_2 Brayton cycle with STP systems. Firstly, the single sCO_2 cycle cannot achieve optimal thermal conversion efficiency in such a wide temperature range of 200~700℃. The sCO_2 cycle only can exhibit cycle efficiency superiority at a high temperature above 500℃ compared with steam Rankine cycle. In addition, the exhaust temperature of the gas turbine in the sCO_2 cycle is high. After being cooled in the regenerator, residual thermal energy is directly cooled by the cooler to the surroundings, causing a large amount of energy loss and significant efficiency decrease.

Furthermore, the regenerator outlet temperature (namely receiver inlet temperature) is high for a simple Brayton cycle, resulting in the high operating temperature of the solar receiver. Actually, the solar-thermal efficiency of the tower receiver is strongly dependent on the receiver temperature. The convection and radiation heat losses of the tower receiver significantly increase with the elevation of the receiver operating temperature.

Finally, at present there is no mature technology for higher temperature thermal storage, and the application of supercritical carbon dioxide in a tower power station is thereby restricted. The MS is regarded as an ideal thermal storage fluid, which has been employed in commercial CSP plants. However, the current MS cannot withstand temperature of above 600℃[24], MS cannot meet the requirement of the higher temperature thermal storage of the sCO_2 systems. Meanwhile, the temperature difference across the solar receiver of the traditional system is also narrow, which causes great challenges for coupling with the sensible thermal energy storage (TES)[25]. Therefore, at the current stage, it is a crucial issue to build a novel sCO_2 cycle layout that can lead to a high efficiency, large specific work, and wide temperature difference across the receiver if the mature sensible TES is going to be adopted.

In this study, a novel solar tower power system integrating with supercritical carbon dioxide Brayton-steam Rankine power cycle is proposed. The power block consists of a top sCO_2 Brayton cycle and bottom steam Rankine cycle. The high temperature exhaust gas of the sCO_2 turbine is introduced to the sCO_2/water heat exchanger for heating subcooling water and generating high temperature and pressure steam, then driving the bottom steam Rankine cycle. The solar tower receiver of the proposed system includes two HTF loops, namely the MS loop and sCO_2 loop, and the lengths of the two loops can be adjusted. The cooled sCO_2 is directly heated by the solar receiver. The MS is regarded as a sCO_2 preheating fluid and thermal storage medium. The current study firstly develops a comprehensive numerical model that involves solar energy collecting subsystem and power cycle subsystem and the overall performance of the solar power systems is evaluated. The cycle efficiency and parameters of the power cycle are analyzed and compared under different design temperatures and pressure. Furthermore, the comparisons of the exergy loss and electricity output between simple sCO_2 and sCO_2-SR systems at design point are carried out.

2. System description

The novel STP system in the present work mainly consists of a solar field, a central tower receiver, a two-tank MS thermal energy storage subsystem, and a cascade sCO_2-RC cycle. The external central tower receiver consists of several solar panels as shown in **Figure** 1a and **Figure** 1b. The receiver is divided into two fluid sections for the STP system as shown in **Figure 1c**, namely the MS loop and sCO_2 loops. The MS and sCO_2 loops are arranged at different positions of the receiver. The loop lengths of the sCO_2 and MS loops are regarded as controllable to match the energy demand in different operating conditions.

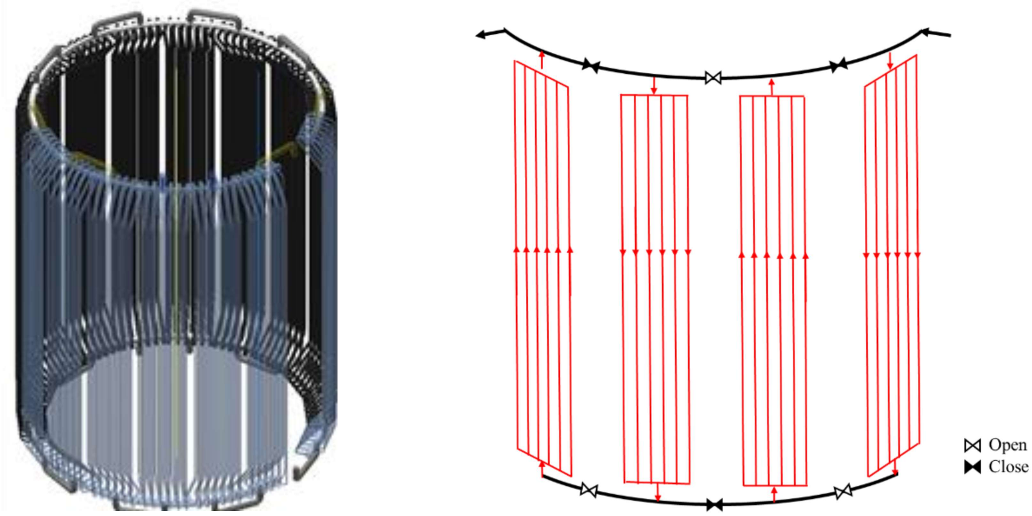

（a） （b）

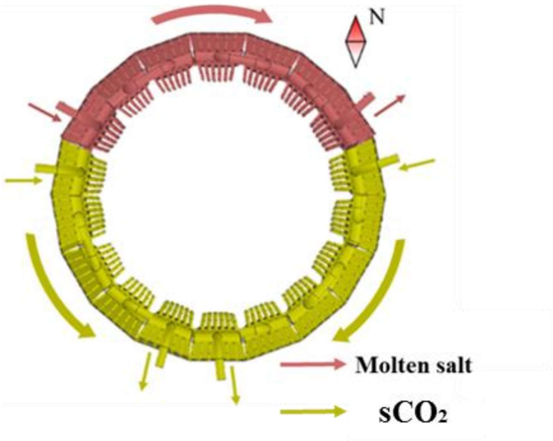

Figure 1 Physical structure of the central receiver's（a）3D view（b）heat transfer fluid flow path of the single fluid reciever (c) the top view of the dual fluid receiver

The operation strategy of the novel cascade STP system can be illustrated as follows

a. When the solar energy gain from the tower receiver can satisfy the full-load operation of the sCO_2 cascade cycle, the sCO_2 from the power block is heated to the desired temperature directly in the tower receiver. The high temperature and pressure sCO_2 is introduced into the turbine for electricity generation. Meanwhile, the energy of the high temperature exhaust gas of the top sCO_2

Brayton cycle is released to the bottom steam Rankine cycle by several sCO_2/water heat exchangers. The sCO_2 and MS loop lengths and mass flow rate of MS are are adjusted according to the solar flux distribution of the receiver to keep full-load operation of the power block. The extra solar energy that exceeds the demand of the power block is collected by the MS loop and stored in the TES subsystem. The diagram of the this operation mode is shown in **Figure 2a**.

b. The energy gain from the receiver is less than the rated heat input to the cascade sCO_2-RC, but the system can still operate at full-load condition if sCO2, prior to its entrance to the receiver, is preheated by molten salts in the heat exchanger. In this case, the sCO_2 is firstly preheated by solar salt from the hot MS tank. Then, the preheated sCO_2 is introduced into the tower receiver to absorb solar irradiation and elevate temperature. Finally, the high temperature and pressure sCO_2 flows into the turbine and generates electricity. The energy of the high-temperature exhauste gas of top sCO_2 Brayton cycle is used to drive the bottom steam Rankine cycle by several sCO_2/water heat exchangers. The diagram of the this operation mode is shown in **Figure 2b**.

c. If the system cannot operate at full-load condition even CO2 is preheated by the molten salts, then the cascade system is closed and the operation strategy of the system is converted to thermal energy storage mode, meanwhile, the bottom steam Rankine cycle can operate by using MS as a heat source or stop, depending on the grid load. The sCO_2 loop is closed and MS is heated by tower receiver to 565℃ and stored in TES subsystem. The diagram of this operation mode is shown in **Figure 2c**.

d. At night or no sun periods, solar energy collecting subsystem, including solar field and tower receiver, is closed. The bottom steam Rankine cycle can keep running. The subcooled water is preheated, evaporated, superheated by hot MS from TES system.

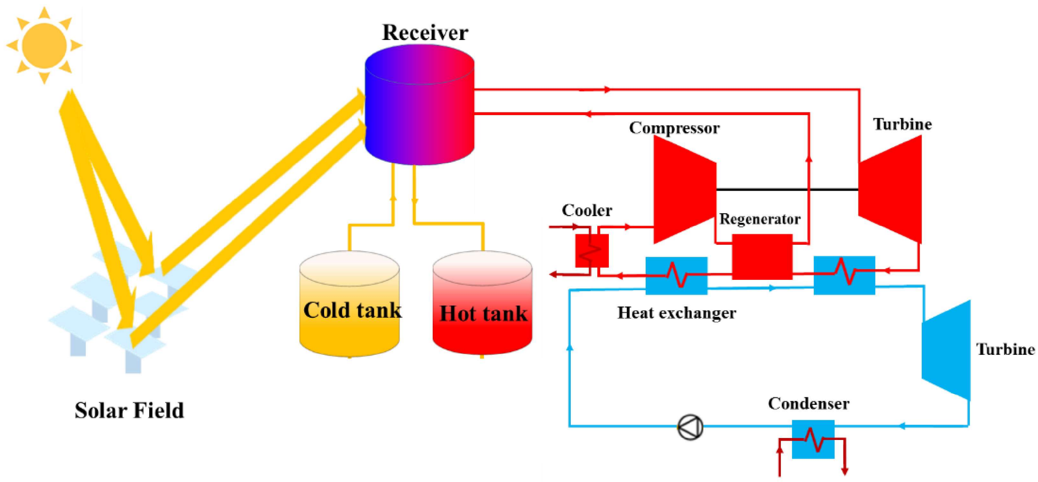
Receiver
Compressor
Turbine
Cooler
Regenerator
Cold tank
Hot tank
Heat exchanger
Turbine
Solar Field
Condenser

(a)

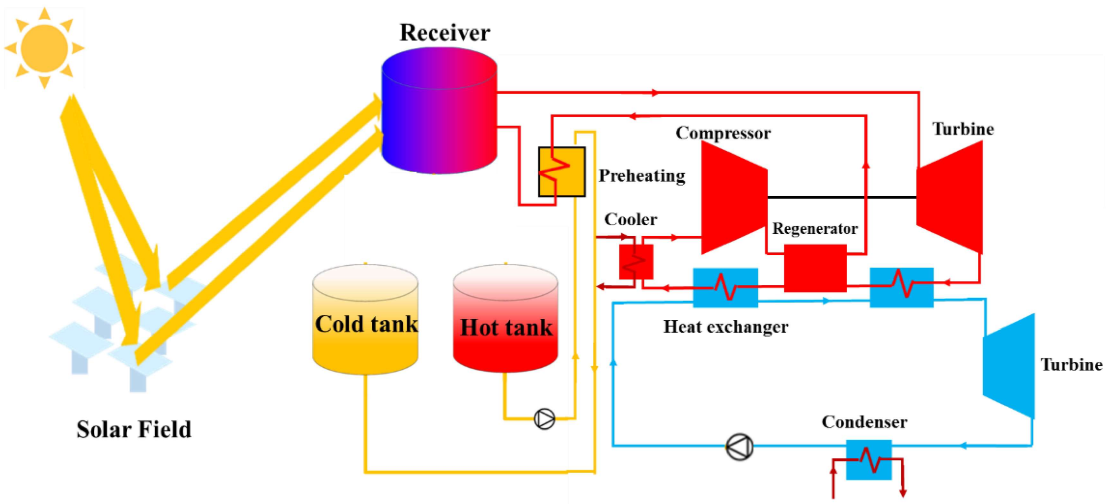
Receiver
Compressor
Turbine
Preheating
Cooler
Regenerator
Cold tank
Hot tank
Heat exchanger
Turbine
Solar Field
Condenser

(b)

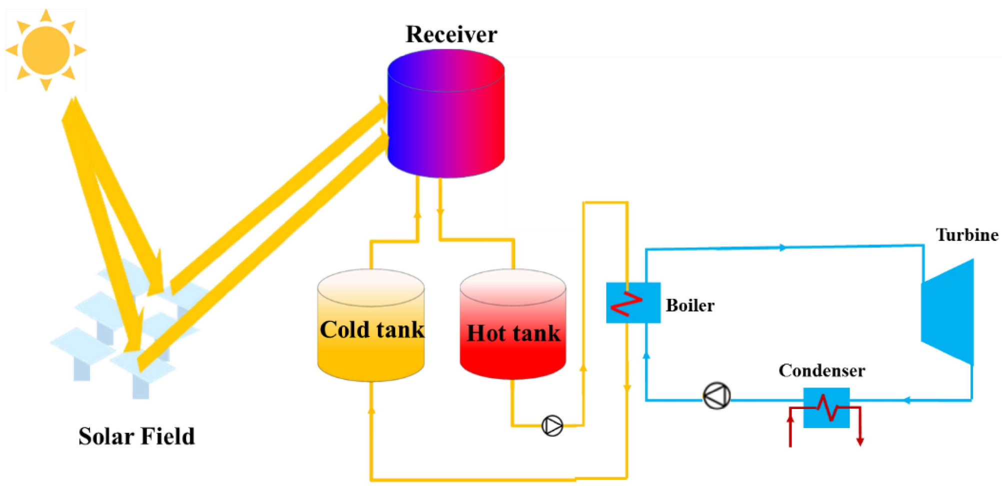
Receiver
Turbine
Boiler
Cold tank
Hot tank
Condenser
Solar Field

(c)

Figure 2 The diagram of the cacasde sCO_2-SR solar power system.(a) full-load operation with thermal storage；(b) full-load operation with molten salt preheating；(c) bottom cycle operation

3. Mathematic model

In this section, the comprehensive system numerical model, including a solar energy collecting subsystem and power block subsystem, is developed to compare the performance of the STP plants using simple sCO_2 and cascade sCO_2-SR system.

3.1 Solar energy collecting subsystem

The numerical model of the solar energy collecting subsystem includes a solar field optical model and central tower receiver heat transfer model. The configuration parameters of the 10MW demonstrated STP plant in Dunhuang with 15h thermal energy storage capacity and an external central tower receiver is selected for modelling as example[26].

3.1.1 Solar field optical model

The detailed design parameters of the solar tower receiver and solar field of the Dunhuang STP plants are presented in **Table** 1 from the FluxSPT model[26].

Table 1 Detailed configuration parameters of the solar power tower systems

Parameters	Unit	Value
Tower height	m	121.4
Receiver height	m	10.5
Receiver diameter	m	7.3
Panels number	/	18
Coating absorption	/	0.94
Coating emittance	/	0.88

Tube outer diameter	mm	40
Tube wall thickness	mm	1.25(3.5)
Tube number per panel	/	31
Heliostats number	/	1525
Heliostats mirror reflectance	/	0.9

The model developed by Domingo Santana is used to obtain the solar flux distribution and concertation of the tower receiver[27]. The aiming factor is employed to simulate solar flux distribution of the receiver, which is a concept to demonstrate the aiming strategy of the solar tower systems. In this study, the value of the aim factor is set as 2. The solar field heliostat efficiencies and solar flux distribution of the receiver with incident solar irradiation of 900W/m^2 at Spring Equinox noon are presented as **Figure 3.**

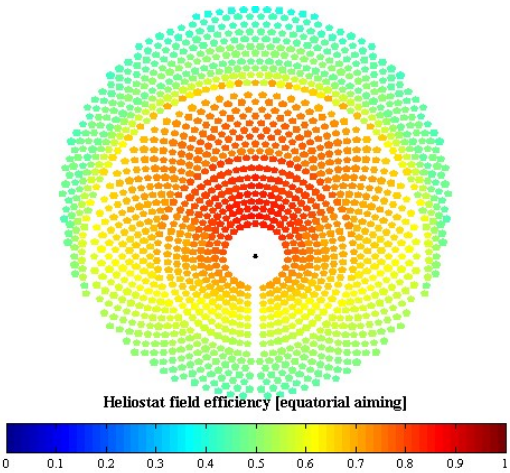

(a)

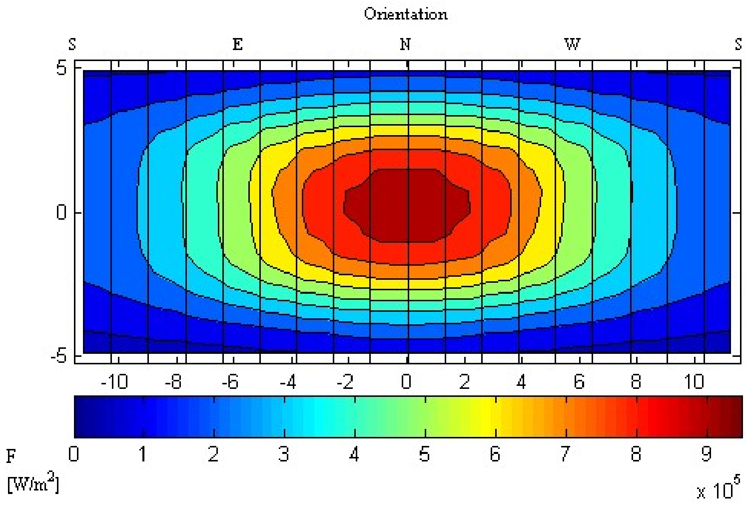

(b)

Figure 3 Optical model of the solar field. (a) heliostat efficiencies at Spring Equinox noon (b) solar flux distribution of the receiver

Then, the solar flux distribution under different solar irradiation conditions at the same time can be calculated as follow:

$$Q_{\mathrm{inf}}\left(i,j\right)=\frac{Q_f\left(i,j\right)Q_{sol}}{900} \tag{1}$$

Where the i and j represents the different positions of the tower receiver ; the $Q_f\left(i,j\right)$ is the solar flux distribution as shown in Figure 2 with the design incident irradiation of 900 W/m^2; Q_{sol} is incident solar radiation that differs from the reference point, W/m^2; Thus the solar flux distribution of the receiver at the different reference point can be obtained by **Equation 1.**

3.1.2 Central tower receiver heat transfer model

The heat transfer model of the central tower receiver is composed of external thermal loss and internal HTF heat transfer. The diagram of the single receiver tube heat transfer is shown as **Figure 4**. The central receiver consists of a large number of single receiver tubes and refractory walls as shown in **Figure 2a.**

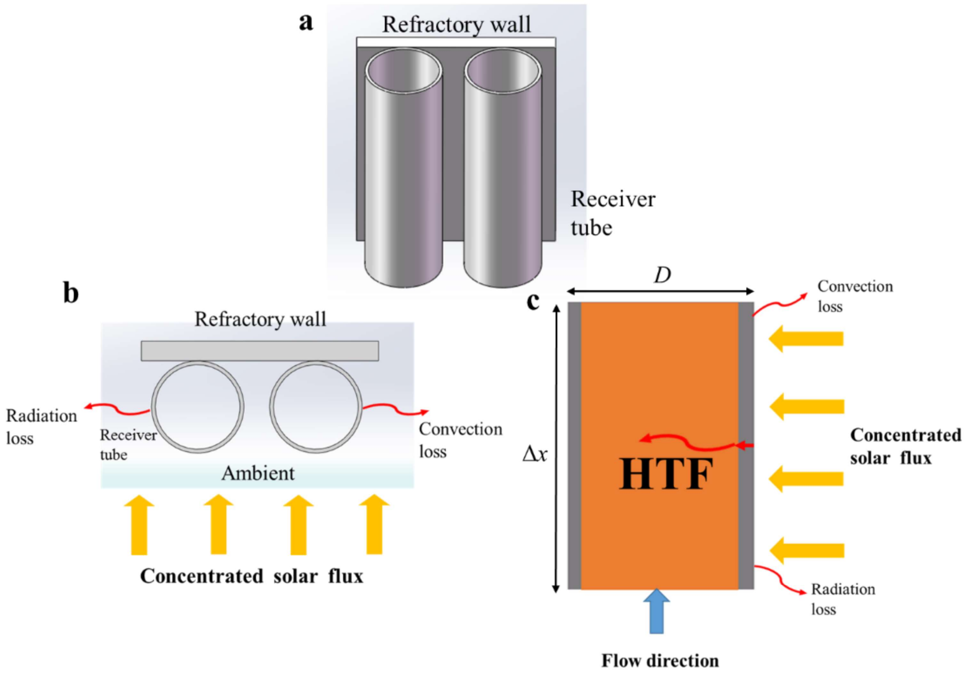

Figure 4 Heat transfer of the central tower receiver. (a) the diagram of the single receiver tube of the tower receiver; (b) external heat loss of the receiver; (c) internal heat transfer of the receiver tube of a control unit.

3.1.2.1 External heat transfer of the receiver tube

The external heat transfer process of the receiver includes radiation, convection heat loss, and solar energy absorption. The external heat transfer of the tower receiver is depicted in **Figure 4b.**

The solar energy absorbed by the receiver can be inferred from solar flux distribution and geometry dimension of the receiver tube as **Equation** (2):

$$Q_{abs} = \alpha Q_{\text{inf}}\left(i,j\right) D\Delta x \tag{2}$$

Where the α is solar irradiation absorption of the solar selective coating; D is the outer diameter of the single receiver tube, m; Δx is length of the receiver tube as shown in **Figure 4c**, m.

The temperature of the receiver tube is regarded as uniform in circumferential and axial directions in a control unit for radiation and convection heat loss calculation. Furthermore, the temperature of the different receiver tubes in a panel is also regarded as uniform in the horizontal direction. Thus, the temperature of the receiver tube varies only in the HTF flow direction. The radiation heat loss calculation of the receiver tube is simplified as two long parallel cylinders. The radiation loss of the receiver is the heat transfer between receiver tube and ambient and is expressed as follows[28]:

$$Q_{loss,r} = \frac{\sigma\left(T_{abs,o}^{4} - T_{0}^{4}\right)}{\frac{1-\varepsilon}{\varepsilon_{abs}A} + \frac{1}{AF}} \tag{3}$$

Where $T_{abs,o}$ is the outer surface temperature of the single receiver tube, K; T_0 is surrounding temperature, K; A is the surface area of the receiver tube, m^2; ε_{abs} is the emissivity of the receiver tube; F is view factor between receiver tube and ambient which can be calculated using Crossed-String method by Modest[29].

The convection heat loss is calculated by Newton cooling formula as follow[28]:

$$Q_{loss,c} = h_c A\left(T_{abs,o} - T_a\right) \tag{4}$$

According to Siebers and Kraabel research[30], the convective heat transfer coefficient h_c of the central external receiver has taken into consideration of the combined action of the forced and natural convective of the air and calculated as follow:

$$h_c = \left(h_{fc}^{3.2} + h_{nc}^{3.2}\right)^{1/3.2} \tag{5}$$

Where natural convective coefficient h_{nc} can be expressed:

$$h_{nc} = \frac{\lambda_a Nu_{nc}}{H} \tag{6}$$

$$Nu_{nc} = 0.049\pi Gr_{nc}^{1/3}\left(\frac{T_a}{T_{abs}}\right)^{0.14} \tag{7}$$

$$Gr_{nc} = \frac{g\beta\left(T_{abs} - T_a\right)H^3}{v_a^2} \tag{8}$$

And the forced convection coefficient h_{fc} is given as:

$$h_{fc} = \frac{\lambda_{a,b} Nu_{fc}}{D_r} \tag{9}$$

$$Nu_{fc} = 0.0455 \mathrm{Re}_{fc}^{0.81} \tag{10}$$

Where H and D_r is the height and diameter of the receiver, respectively. The volumetric thermal expansion coefficient β is equal to $1/T_a$ for the air and the kinematic viscosity of the air ν_a is evaluated at the ambient temperature T_a. $\lambda_{a,b}$ is evaluated at the arithmetic average of the tube temperature and the ambient temperature while the thermal conductivity for the natural convection λ_a is evaluated just at the ambient temperature.

3.1.2.2 Internal heat transfer of the receiver tube

In this work, the sCO_2 and MS are employed as HTF to deliver thermal energy to the power block. The heat flux of the HTF heat transfer is expressed by Newton cooling formula[28]:

$$Q_{conv} = \pi h_f D_{abs,i} \left(T_{abs,i} - T_f \right) \tag{11}$$

$$h_f = Nu_f \frac{k_f}{D_{abs,i}} \tag{12}$$

where Q_{conv} is the convection heat flux between absorber inner surface and HTF, W; h_f is the heat convection transfer coefficient, W/(m^2·K); $D_{abs,i}$ is the inner diameter of the absorber tube, m; $T_{abs,i}$ and T_f are the temperatures of inner surface of the absorber tube and HTF, °C; and k_f is the thermal conductance of the HTF, W/(m·K). The sCO_2 and MS are regarded as single-phase fluid, thus the Nusselt number of the internal flow for transitional and turbulent flow can be calculated by Gnielinski formula[28]:

$$Nu_f = \frac{f_{abs,i}/8 \left(\mathrm{Re}_f - 1000 \right) \mathrm{Pr}_f}{1 + 12.7 \sqrt{f_{abs,i}/8} \left(\mathrm{Pr}_f^{2/3} - 1 \right)} \left(\frac{\mathrm{Pr}_f}{\mathrm{Pr}_{abs,i}} \right)^{0.11} \tag{13}$$

$$f_{abs,i} = \left(1.82 \log_{10} \left(\mathrm{Re}_f \right) - 1.64 \right)^{-2} \tag{14}$$

where $f_{abs,i}$ is the friction factor for the inner surface of the absorber tube; $\Pr_f$ and $\Pr_{abs,i}$ are the Prandtl numbers of the HTF evaluated at the HTF temperature and absorber inner surface temperature. The thermophysical property of the sCO_2 is acquired by means of commercial software RefProp 9.1[31] and that of the MS is obtained by the empirical formula presented in reference[32].

The conduction heat transfer of the receiver tube wall can be obtained by the Fourier's law of hollow cylinder [28]:

$$Q_{cond} = \frac{2\pi\lambda\left(T_{abs,i} - T_{abs,o}\right)}{\ln\left(\frac{D_{abs,o}}{D_{abs,i}}\right)}, \tag{15}$$

where λ is the thermal conductivity of the receiver tube wall, W/(m·K).

Based on above external and internal heat transfer of the receiver tube, the receiver tube is divided into a number of the control volume unit with an interval length of 0.1m along the HTF flow direction, thus the mass flow rate of the HTF is obtained with the given outlet temperature and solar irradiation by solving control unit energy balance equation:

$$m\left[c_{p,j}\left(T_{in,j} - T_{out,j}\right) + \frac{1}{2}\left(v_{in,j}^2 - v_{out,j}^2\right)\right] + Q_{abs,j} - \Delta x\left(Q_{loss,r,j} + Q_{loss,c,j}\right) = 0 \tag{16}$$

where Δx is the length of the control volume unit, m. The outlet temperature of the "j" control volume unit is set as inlet temperature of the "j+1" control volume unit. The iteration is performed similarly until a loop cycle of the receiver pipeline is finished. The calculation processes and flow chart of the numerical model for different operation strategies are described in **Appendix**.

3.2 Thermodynamics model of the power cycle

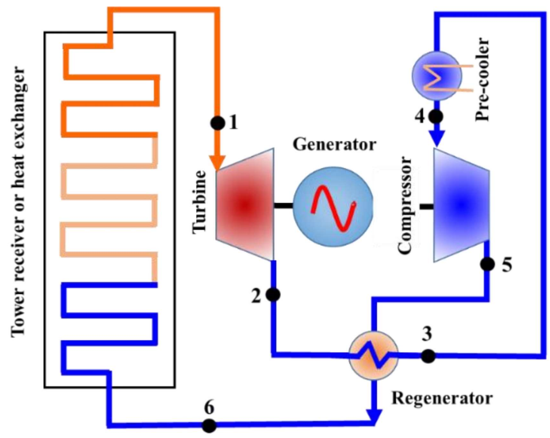

a

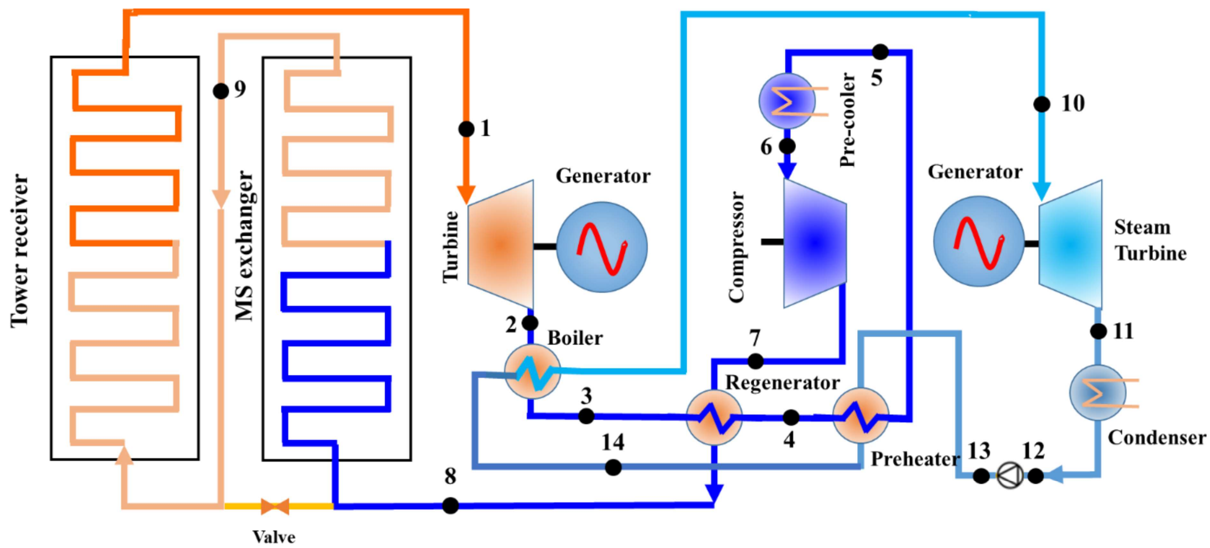

b

Figure 5 The diagram of the power cycle (a) simple Brayton cycle (b) cascade sCO_2-SR cycle using MS preheating

Table 2 Input parameters of the power cycle[19]

Input parameters	Value
Maximum sCO_2 cycle pressure, P_{max}	20~35 MPa
Minimum sCO_2 cycle pressure, P_{min}	7.36 MPa
sCO_2 Compressor inlet temperature, T_{cci}	32 ℃

Gas turbine inlet temperature, T_{cti}	550~900℃
Turbine isentropic efficiency, η_t	0.93
Compressor isentropic efficiency, η_c	0.89
Steam condenser pressure, P_{sto}	8 kPa

Table 3 Energy balance of the power cycle[33]

Component	Simple Bayton cycle	Cascade cycle
sCO_2-Compressor	$\eta_c=(h_{5s}-h_4)/(h_5-h_4)$	$\eta_c=(h_{7s}-h_6)/(h_7-h_6)$
	$W_{cc}=m_c(h_5-h_4)$	$W_{cc}=m_c(h_7-h_6)$
Water pump	/	$W_{sc}= m_s(h_{13}-h_{12})$
sCO_2-Turbine	$\eta_t=(h_1-h_2)/(h_1-h_{2s})$	$\eta_t=(h_1-h_2)/(h_1-h_{2s})$
	$W_{ct}=m_c(h_1-h_2)$	$W_{ct}=m_c(h_1-h_2)$
Steam-Turbine	/	$\eta_t=(h_{10}-h_{11})/(h_{10}-h_{11s})$
	/	$W_{st}=m_c(h_{10}-h_{11})$
Regenerator	$h_2-h_3=h_6-h_5$	$h_3-h_4=h_8-h_7$
Preheater	$m_c(h_4-h_5)= m_s(h_{13}-h_{13})$	/
Biloer	$m_c(h_2-h_3)= m_s(h_{10}-h_{14})$	/
Heat source	$Q_c=m_c(h_1-h_6)$	$Q_c=m_c(h_1-h_8)$

Table 4 Exergy analysis of the power plant

Component	Simple Bayton cycle	Cascade cycle
Solar field	$Ex_s=\eta_s N A_m Q_f$	$Ex_s=\eta_s N A_m Q_f$
	$\eta_s=1-\frac{4}{3}\frac{T_a}{T_{sun}}+\frac{1}{3}\left(\frac{T_a}{T_{sun}}\right)^4$	$\eta_s=1-\frac{4}{3}\frac{T_a}{T_{sun}}+\frac{1}{3}\left(\frac{T_a}{T_{sun}}\right)^4$

Receiver surface	$Ex_r=\eta_s A_r Q_{inf}$	$Ex_r=\eta_s A_r Q_{inf}$
	$\eta_s = 1 - \frac{4}{3}\frac{T_a}{T_{sun}} + \frac{1}{3}\left(\frac{T_a}{T_{sun}}\right)^4$	$\eta_s = 1 - \frac{4}{3}\frac{T_a}{T_{sun}} + \frac{1}{3}\left(\frac{T_a}{T_{sun}}\right)^4$
HTF	$\Delta Ex_h = m_c\left[\left(h_6 - h_1\right) - T_a\left(s_6 - s_1\right)\right]$	$\Delta Ex_h = m_c\left[\left(h_8 - h_1\right) - T_a\left(s_8 - s_1\right)\right]$
sCO_2-Turbine	$\Delta Ex_{ct} = m_c\left[\left(h_1 - h_2\right) - T_a\left(s_1 - s_2\right)\right]$	$\Delta Ex_{ct} = m_c\left[\left(h_1 - h_2\right) - T_a\left(s_1 - s_2\right)\right]$
sCO_2-Compressor	$\Delta Ex_{cc} = m_c\left[\left(h_4 - h_5\right) - T_a\left(s_4 - s_5\right)\right]$	$\Delta Ex_{cc} = m_c\left[\left(h_6 - h_7\right) - T_a\left(s_6 - s_7\right)\right]$
Regenerator		
High pressure side	$\Delta Ex_{cre,h} = m_c\left[\left(h_5 - h_6\right) - T_a\left(s_5 - s_6\right)\right]$	$\Delta Ex_{cre,h} = m_c\left[\left(h_7 - h_8\right) - T_a\left(s_7 - s_8\right)\right]$
Low pressure side	$\Delta Ex_{cre,l} = m_c\left[\left(h_2 - h_3\right) - T_a\left(s_2 - s_3\right)\right]$	$\Delta Ex_{cre,l} = m_c\left[\left(h_3 - h_4\right) - T_a\left(s_3 - s_4\right)\right]$
Pre-cooler	$\Delta Ex_{cp} = m_c\left[\left(h_3 - h_4\right) - T_a\left(s_3 - s_4\right)\right]$	$\Delta Ex_{cp} = m_c\left[\left(h_5 - h_6\right) - T_a\left(s_5 - s_6\right)\right]$
Steam-Turbine	/	$\Delta Ex_{st} = m_s\left[\left(h_{10} - h_{11}\right) - T_a\left(s_{10} - s_{11}\right)\right]$
Condenser	/	$\Delta Ex_{sd} = m_s\left[\left(h_{11} - h_{12}\right) - T_a\left(s_{11} - s_{12}\right)\right]$
Bioler	/	*Simialr with regenerator*
Preheater	/	*Simialr with regenerator*

For a preliminary demonstration of the advantages of the hybrid systems, a simple Brayton cycle and a cascade cycle based on simple Brayton and Rankine cycle are employed for performance comparison. A simple Brayton cycle consists of a gas compressor, turbine, heat regenerator and precooled exchanger as shown in **Figure 5a**. For the cascade cycle, the system configuration is slightly more complex than that of the simple Brayton cycle as shown in **Figure 5b**. The valve is employed to control sCO_2 preheating according to solar incident irradiation. The input parameters of the two cycle systems are presented in **Table 2[19]**. For the heat exchanger, such as regenerator, boiler, the minimum heat transfer difference are set as 10℃. The energy balance and exergy analysis of the main component of the simple and cascade cycle are listed in **Table 3 and Table 4**. Based on the parameters shown in **Table 3**, the cycle efficiency of the systems can be calculated as follows:

Simple Brayton cycle efficiency:

$$\eta = \frac{W_{ct} - W_{cc}}{Q_c} \tag{17}$$

Cascade cycle efficiency:

$$\eta = \frac{W_{ct} - W_{cc} + W_{st} - W_{st}}{Q_c} \tag{18}$$

The exergy loss of the each components can be also calculated by the exergy and exergy difference results as presented in **Table 4**.

The sCO_2 mass flow rate of a power block can be obtained by following **Equation(19) and Equation(20)** :

Simple Brayton cycle :

$$m_c = \frac{P}{(h_1 - h_2) - (h_5 - h_4)} \tag{19}$$

Cascade cycle:

$$m_c = \frac{P}{(h_1 - h_2) - (h_7 - h_6) + x\left[(h_{10} - h_{11}) - (h_{13} - h_{12})\right]} \tag{20}$$

$$x = \frac{\left[(h_2 - h_3) + (h_4 - h_5)\right]\eta_T}{h_{10} - h_{13}} \tag{21}$$

Where P is net work output of the power block, W; h_1, h_2, h_4, h_5, h_6, h_7, h_{10}, h_{11}, h_{12} and h_{13} are the enthalpy of the fluid at different points; x is ratio of the steam mass flow to carbon dioxide mass flow; η_T is thermal efficiency of the heat transfer exchangers.

3.3 Model validation

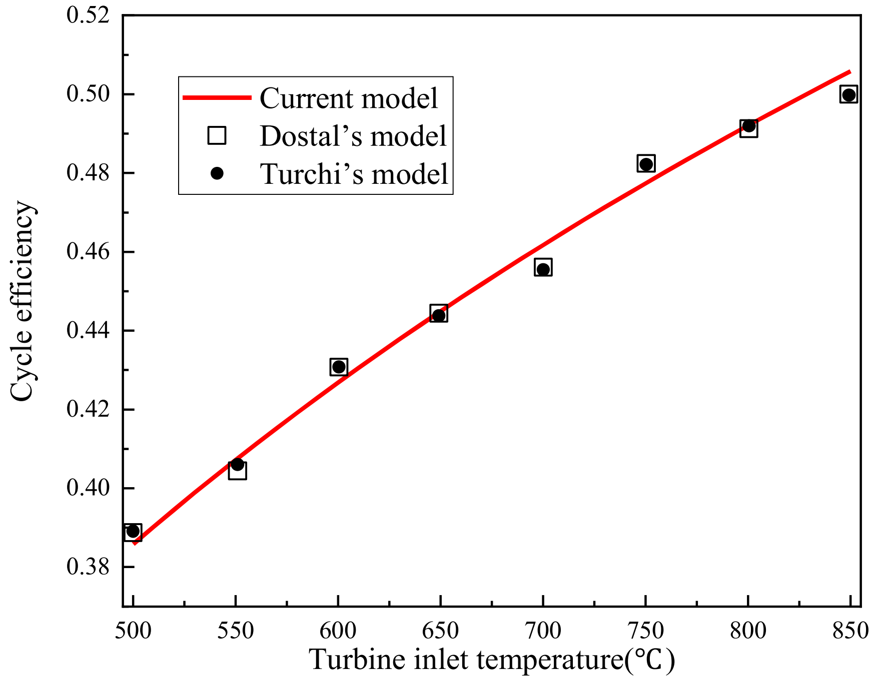

Figure 6 Validation of the power cycle

The simple Brayton cycle is also validated by the previous works with the inlet temperature from 500℃ to 850℃ as shown in **Figure 6**. The relative error between the current model and reference results is between 0.01% and 1.5% for all operation temperatures. The parameters used for model validation are listed in **Table 2.** The HTF heat transfer model and solar field optical model used in this study have been investigated and validated by previous work.[34] Based on the above results of the comprehensive thermodynamic model of the power cycle and validated solar collecting subsystem model, the current numerical model can be extended to overall performance analysis of the solar tower power system integrated with sCO_2 Brayton cycle.

4. Results and discussion

The simulation process is implemented in a Matlab program based on the above model and parameters. The thermodynamics performance analysis and operation strategy adjustment of the soalr power systems are elaborated in this section.

4.1 Thermodynamics analysis

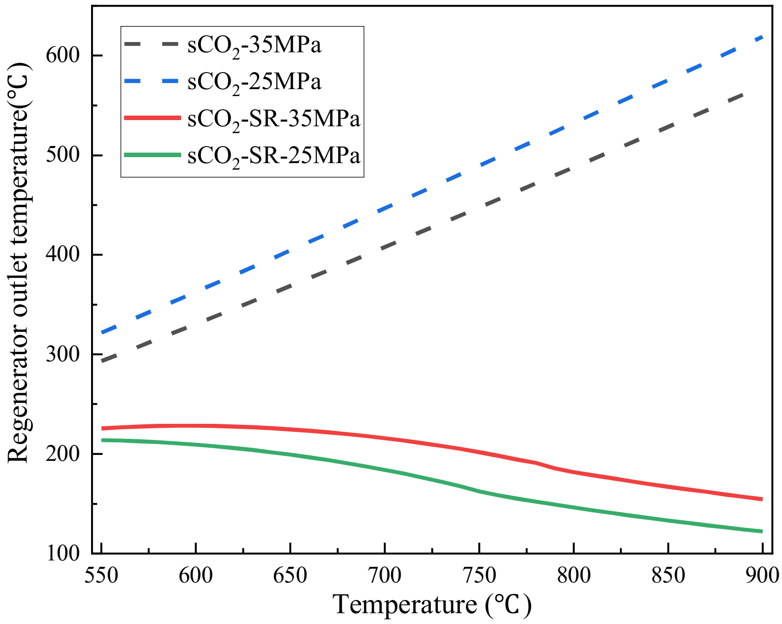

Figure 7 Regenerator outlet temperature variations with the turbine inlet temperature

The solar energy collecting temperature is crucial to solar-thermal conversion efficiency in solar power systems. The regenerator outlet temperature (namely tower receiver inlet temperature) variations with turbine inlet temperature and maximum operation pressure are presented in **Figure 7.** The regenerator outlet temperature of the simple sCO_2 system increases with the turbine inlet temperature but decreases with pressure. The influences of turbine inlet temperature on the two solar systems are different. For the simple sCO2 cycle system, a lower turbine inlet pressure and higher inlet temperature lead to a higher exhaust temperature, resulting in a higher heat regeneration outlet temperature. While for the cascade system, given a constant power output of 10 MW, a higher turbine inlet temperature is accompanied with a larger power put by the SR cycle. More energy is released from the exhaust gas to the bottom SR cycle via the sCO_2/water heat exchanger, leading to a lower heat regeneration outlet temperature.

Notably, the regenerator outlet temperature of the sCO_2-SR cycle is significantly lower than that of the simple sCO_2 cycle, especially at high operating temperature. It indicates that the average solar receiver temperature can be decreased appreciably and the solar-thermal conversion efficiency is also improved. Furthermore, the lower inlet temperature also presents a wide temperature difference across the solar receiver, improving the specific work of the TES system if there is a suitable thermal fluid for thermal storage of the sCO_2 system with a lower HTF flow rate. The challenges of the narrow temperature difference across the solar receiver and low specific work of the TES system of the traditional sCO_2 system are overcome.

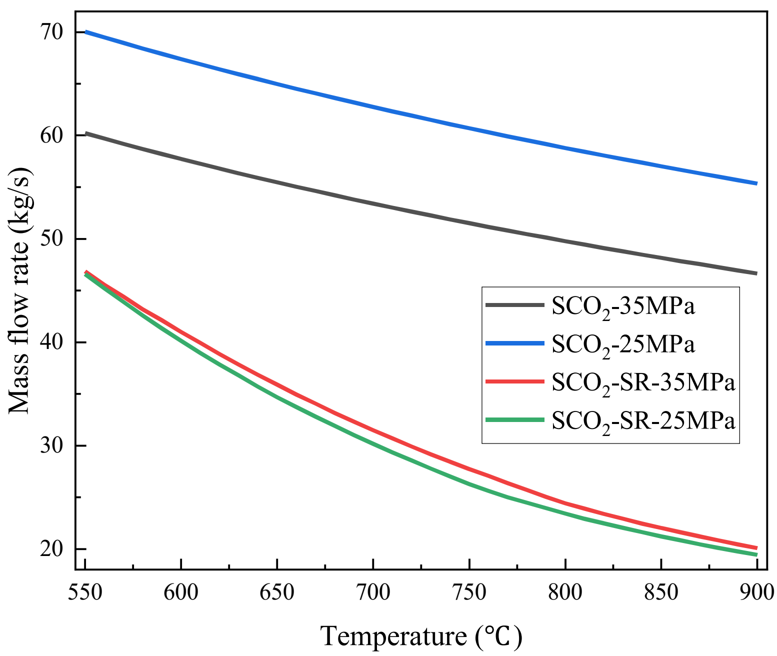

Figure 8 Variation of the sCO_2 mass flow rate with the turbine inlet temperature

The mass flow rate is also a crucial parameter for systems operation. A lower mass flow rate of the working fluid leads to a lower pressure drop in receiver and heat exchanger and more moderate irreversible loss in the compressor and turbine. The variations of the sCO_2 mass flow rate of the 10MW systems with turbine inlet temperature are presented in **Figure 8**. The mass flow rate of the working fluid decreases with the elevation of the turbine inlet temperature for all cases. The mass flow rate of the cascade systems is lower than that of the simple systems at the same turbine inlet temperature and pressure. It decreases from 46.9kg/s at 550℃ to 20.1kg/s at 900℃ with the inlet pressure of 35MPa, while for the simple sCO_2 system, it drops from 60.2 kg/s to 46.7 kg/s. Furthermore, the sCO_2 mass flow rate of the cascade system is not sensitive to turbine inlet pressure. The difference of the flow rates at 25 and 35 MPa is less than 2.0 kg/s at a given temperature for cascade system. While the difference is more remarkable for the simple sCO_2 system, which is approximately 10kg/s in the simulation temperature range.

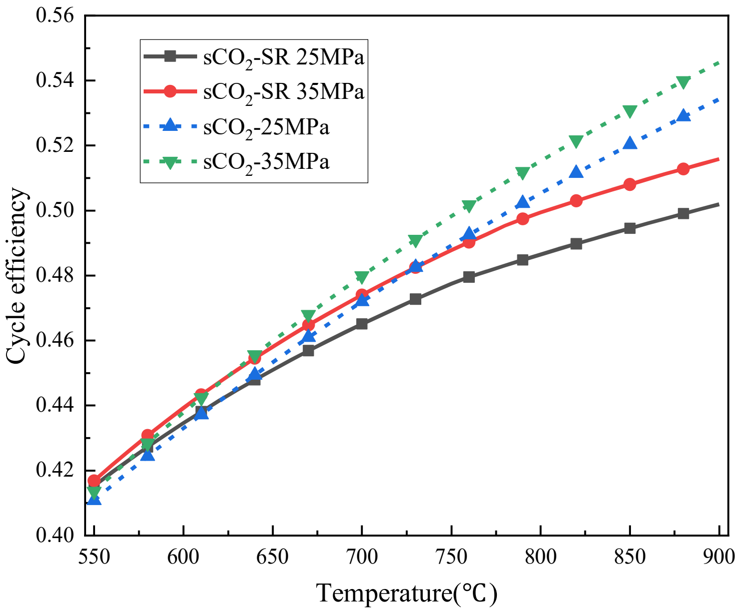

Figure 9 Cycle efficiency variations of the power block subsystems with the turbine inlet temperature

The cycle efficiency variations with turbine inlet temperature from 550℃ to 900℃ and pressure from 25MPa to 35MPa are presented in **Figure 9.** The cycle efficiencies both for sCO_2 and sCO_2-SR cascade systems increase with turbine inlet temperature and pressure. The cycle efficiency is elevated from 41.4% to 53.4% when the inlet temperature increases from 550℃ to 900℃ at inlet pressure of 25MPa and it is improved from 53.4% to 54.6% with the pressure from 25MPa to 35MPa at 900℃ for simple sCO_2 cycle. By comparing the results for sCO_2 and sCO_2-SR systems, it is indicated that the cycle efficiency of the sCO_2-SR cascade cycle is firstly higher than that of the simple sCO_2 system when the temperature is below 630℃. The sCO_2-SR system shows a poorer performance at the temperature higher than 630℃ in terms of power conversion. It can be explained by the inferior thermodynamic performance of the steam Rankine cycle and lower thermal grade of the sCO_2-SR system due to the lower average endothermic temperature of the receiver. Less exhaust thermal energy and lower exhaust temperature of the sCO_2-SR system at operation temperature can compensate for the higher irreversible losses of steam Rankine cycle and lower thermal grade of the cycle fluid, then presenting higher comprehensive cycle efficiency.

To explore the contribution of the power cycle subsystem and solar energy collecting subsystem on the overall performance of systems, the heat gains of the tower receiver for two system configurations are presented in **Figure 10** at noon on the spring equinox in Dunhuang with the incident solar irradiation of 700W/m^2. The heat gain of two systems decreases with the increase of the turbine inlet temperature. The heat gain of the sCO_2-SR system is significantly higher than that of simple sCO_2 system at high temperature. It can be explained by the lower operation temperature of the tower receiver as shown in **Figure 7**. The heat gains of the tower receiver for simple sCO_2 and cascade sCO_2-SR systems are 46.3 MWh and 53.4 MWh at the receiver outlet temperature of 900℃ and pressure of 35MPa, respectively. The influences of the operation pressure on heat gain of the two systems are different. A higher outlet pressure tends to lower heat gain for the cascade system, which is caused by the lower average solar tower receiver operation temperature described in **Figure 10.** The results indicate that the proposed cascade system is promising in improving thermal conversion efficiency of solar tower power technology.

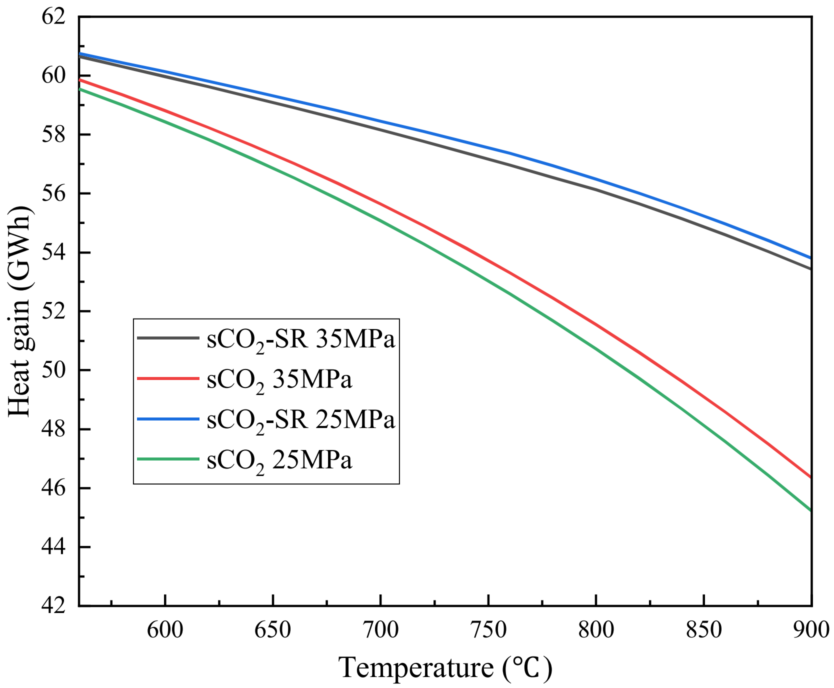

Figure 10 Heat gain of the solar tower receiver

In order to further study the thermodynamic irreversibility of the system, the irreversible loss of the solar power systems can be divided into six parts associated with the solar field, solar tower receiver, turbine, compressor, cooler, sCO_2 heat exchangers. The losses of the sCO_2 heat exchangers cover all exergy destruction in exhaust gas heat exchangers, including water preheater, regenerator, and boiler as shown in **Figure 5**. Based on the aforementioned model and analysis, the exergy loss for the energy conversion process is presented in **Figure 11** at a sCO_2 turbine inlet temperature of 900℃. It can be observed that the solar field optical loss and photo-thermal conversion of the tower receiver are the two biggest exergy losses of the systems. The exergy losses of the solar field for two systems are the same. The exergy loss of the receiver of the cascade system is slightly higher than that of the simple sCO_2 cycle. For the power cycle subsystem, the exergy losses of the compressor, cooler, regenerator of the proposed cascade sCO_2-SR systems are lower than those of the simple sCO_2, while the reverse is true for the turbine, heat exchangers and additional bottom cycle are the opposite of aforementioned results.

The phenomenon of the above exergy loss destruction will be explained one by one. The exergy loss of the receiver is increased from 38 MWh to 38.7 MWh. The reason for this phenomenon is that the higher conversion efficiency of the cascade system receiver cannot compensate for the lower exergy of working fluid resulting from the lower average temperature of the HTF. The sCO_2 possesses more superior thermodynamics performance compared to the steam under current operation temperature, resulting in a higher turbine loss of the proposed system. As shown in **Section 4.1**, the lower mass flow rate of the sCO_2 in sCO_2-SR system leads to lower exergy loss of the sCO_2 compressor. Moreover, the state of work fluid of the bottom cycle is liquid during compression; the exergy loss of pump is significantly lower than that of the compressor. Thus, the total compressor or pump exergy loss of the sCO_2-SR system is lower than that of the simple sCO_2 system. For cooler exergy loss, the pre-cooler inlet temperature is only 366.0K for the sCO_2-SR system, while the inlet temperature of the simple sCO_2 is 415K. Meanwhile, the condenser temperature of the Rankine cycle is only 309K, thus the total exergy loss of the cooler (includes pre-cooler and condenser) of the sCO_2-SR system is significantly lower than that of the simple sCO_2 system due to a lower exhaust gas temperature. The sCO_2-SR system has a better temperature match and lower heat transfer temperature difference in the regenerator and boiler, leading to a lower exergy loss in the sCO_2 exchanger.

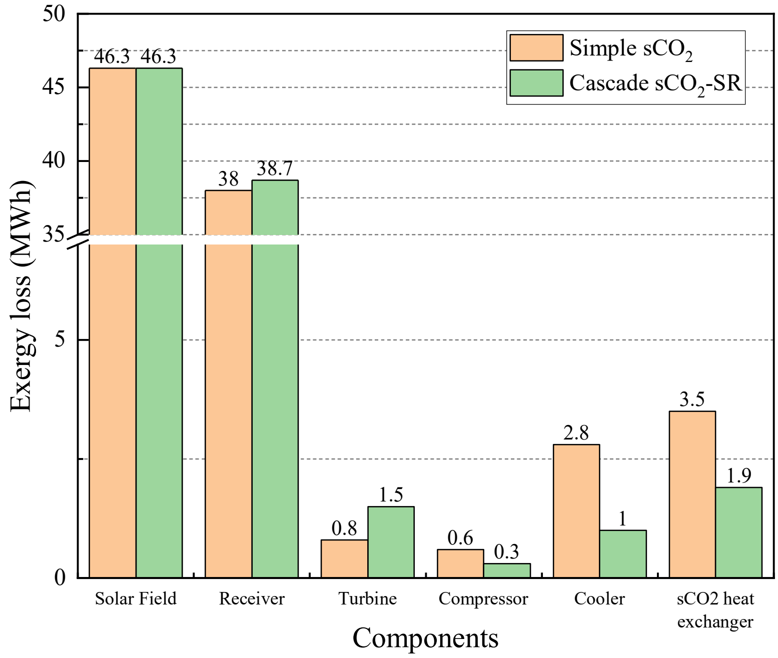

Figure 11 Exergy loss of the solar tower power systems

4.2 Performance analysis of the power plants

The operation parameters of the solar power system, including operation temperature, pressure and solar irradiation, are the critical parameters to overall performance of the power system. The influences of the aforementioned parameters on system performance are illustrated in this subsection.

4.2.1 Operation temperature and pressure

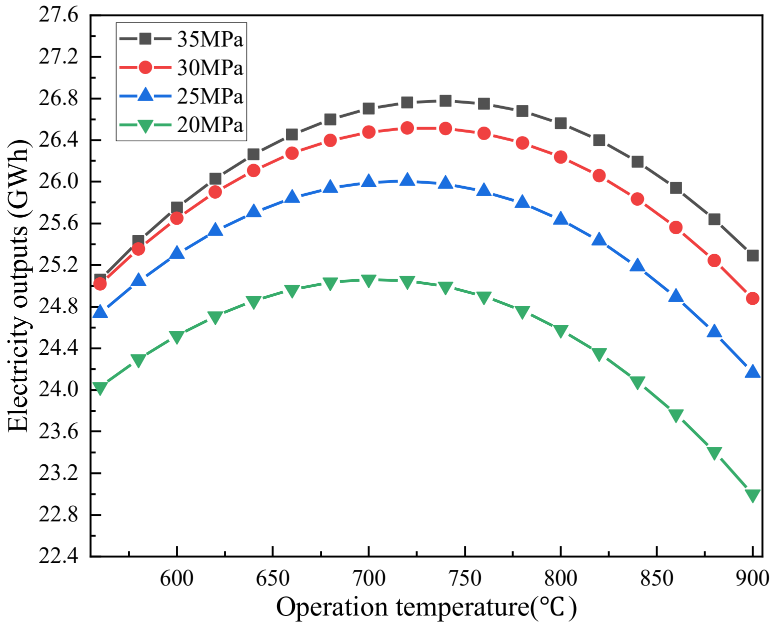

(a)

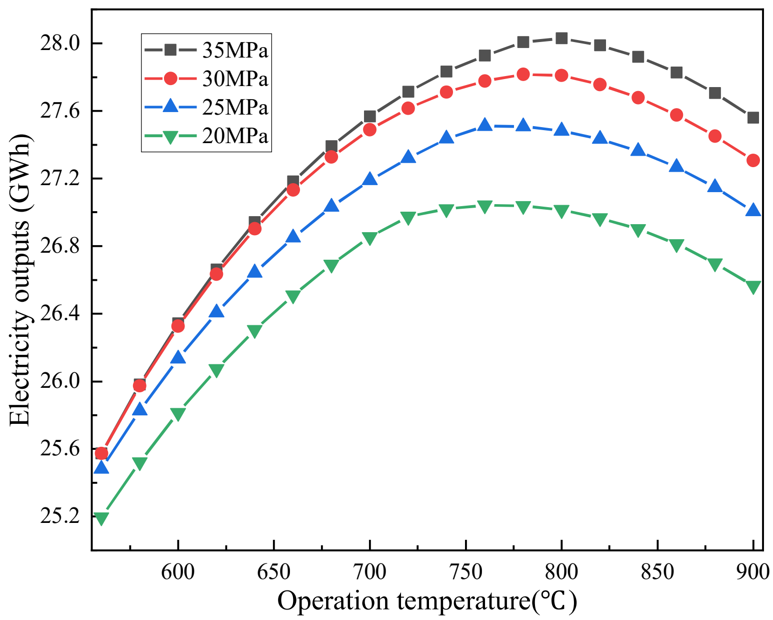

(b)

Figure 12 Electricity production of the power plants with different operating temperature and pressure. (a) simple sCO_2 system (b) cascade sCO_2-SR system

To illustrate the overall performance of the simple sCO_2 and sCO_2-SR cascade cycle, including the solar energy collecting subsystem, the electricity productions at noon on the summer solstice in

Dunhuang with the incident irradiation of 700W/m^2 are analyzed as shown in **Figure 12.** The results show that the electricity productions have the bell curve with a maximum value at the turbine inlet temperature of 700~750℃ for simple sCO_2 systems and 750~800℃ for cascade system. The electricity production and optimal temperature of the solar power systems are affected by the thermal efficiency of the receiver and power cycle efficiency simultaneously. Solar power system performance at high temperature is strongly dependent on the exergy loss of solar energy collecting subsystems, particularly in solar receiver due to significantly increased convection and radiation heat losses. The proposed sCO_2-SR system possesses lower average receiver operation temperature, thus the positive contribution of the solar thermal efficiency improvement of the receiver has overpassed the negative effect of lower power cycle efficiency, leading to higher electricity production and optimal temperature. The electricity productions of the simple sCO_2 system and sCO_2-SR cascade system are 25.2 MWh and 27.6 MWh at the turbine inlet temperature of 900℃ and pressure of 35MPa under design condition. The electricity production of the cascade system is improved by 9.5%. The electricity productions increase with the increase of the maximum operation pressure for both the simple sCO_2 and sCO_2-SR cascade cycle, but the impact is more appreciable in a lower pressure range. It indicates that the turbine inlet pressure possesses a stronger effect on overall performance especially at low pressure conditions.

4.2.2 Solar irradiation

Solar radiation is constantly changing throughout the year. Thus, solar irradiation plays an important role in overall performance and optimum operating temperature. The ratio of electricity production to the maximum electricity production W/W_{max} from 560℃ to 900℃ is selected as evaluation parameters to demonstrate the performance of the system under different temperatures and solar irradiation condition. The $\boldsymbol{W/W_{max}}$ of the two systems is presented in **Figure 13** with the turbine inlet pressure of 35MPa. The peak electricity production temperatures increase with the increase of solar radiation both for two systems. The temperature of peak electricity production of the simple sCO_2 system is 580℃, 680℃, 740℃, 800℃ when the corresponding incident solar irradiation is 300W/m^2, 500W/m^2, 700W/m^2, 900W/m^2. While the peak electricity output occurs at 640℃, 740℃, 800℃, 820℃ for the cascade system. The reason for this phenomenon is that the power cycle efficiency improvement at high solar incident irradiation can exceed the heat loss attenuation of the tower receiver at high temperature, leading to higher optimal operating temperature. Furthermore, the cascade system presents higher optimal electricity production and slight electricity attenuation when the operation temperature deviates from the optimal temperature, especially at low solar irradiation conditions. The $\boldsymbol{W/W_{max}}$ of the simple sCO_2 cycle decreases from 1 at 580℃ to 0.56 at 900℃ with solar incident irradiation of 300W/m^2, while it only decreases from 1 at 640 ℃ to 0.84 at 900℃ for the cascade system. It is indicated that the cascade systems can exhibit more superior performance at off-optimal operation temperatures compared to simple sCO_2 system. The electricity production improvement of the cascade systems at optimal temperature is only 5.8% with solar incident irradiation of 300W/m^2, while it is 59.0% at 900℃ with solar incident irradiation of 300W/m^2 compared to those of the simple system. Thus, the cascade system can give a more excellent overall performance under various reference solar irradiations.

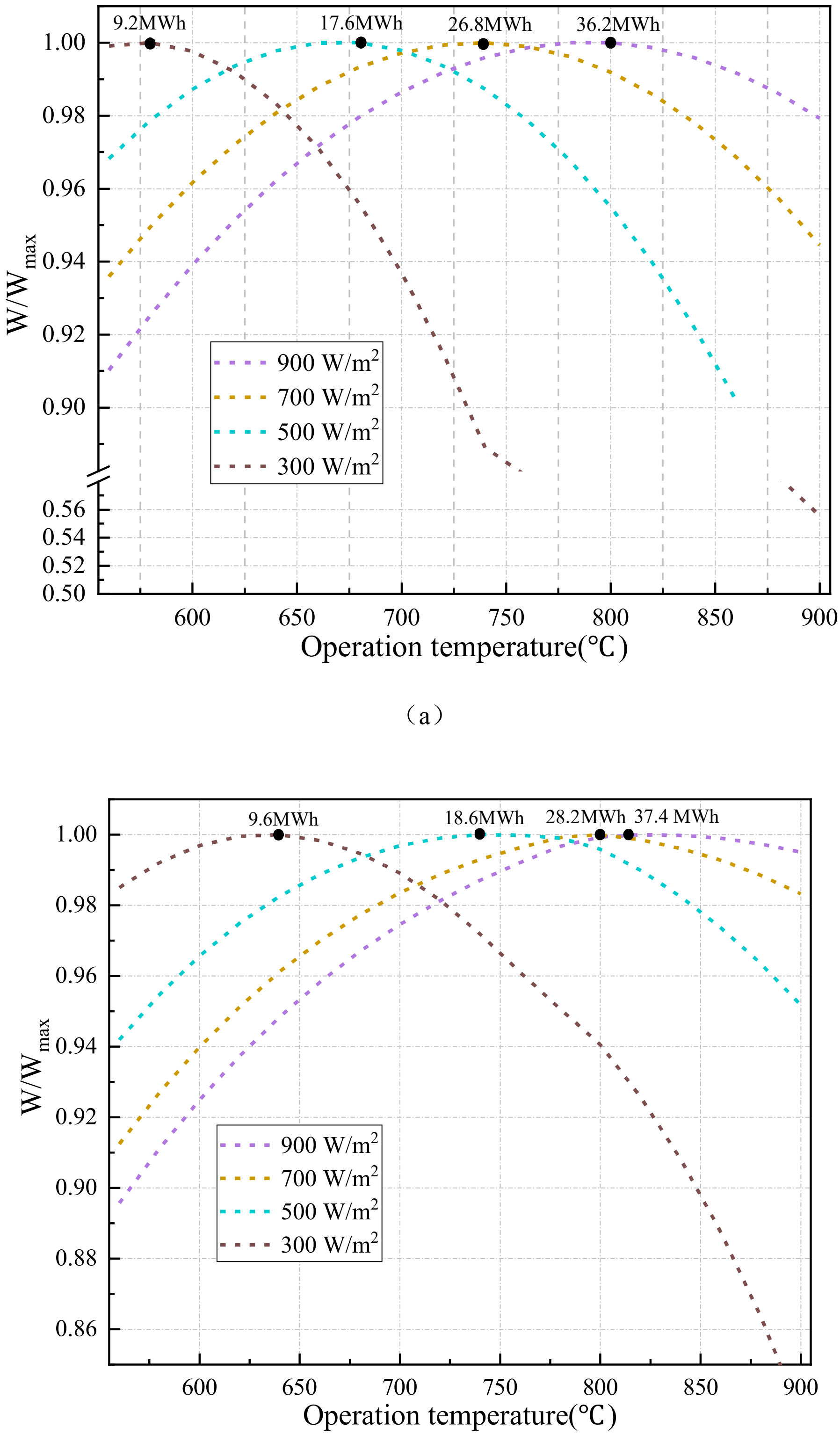

（a）

（b）

Figure 13 The ratio of power generation to the maximum power generation at different temperature at same incident irradiation (a) simple sCO_2 system (b) cascade sCO_2-SR system

4.3 Operation strategy adjustment

The thermal storage system is not considered in aforementioned analysis. Aiming to combine the thermal energy storage subsystem with the sCO_2 solar power system, the MS solar collecting loop is introduced in solar tower receiver and the operation strategy of the cascade solar power system is also analyzed. In this section, the power output of the power block is set as constant. To explore the flexibility of the cascade system, this study assumes that the system can operate at full load when the solar radiation is 500W/m^2 at the design point using single sCO_2 as HTF (i.e. the flow rate of MS in the receiver is 0). If the incident solar irradiation is over 500W/m^2, the sCO_2 and MS loop lengths are adjusted according to the solar flux distribution of the receiver. The extra solar energy that cannot be absorbed by the sCO_2 loop is collected by MS loop and stored in TES subsystem. While, the solar incident irradiation is below 500W/m^2, the HTF of the receiver loop is sCO_2 and its flow rate is set as constant value that is the same as the flow rate under full load operating condition. The solar incident irradiation is not enough to heat HTF to the desired outlet temperature at lower solar irradiation, thus the stored MS is used to preheat sCO_2, then preheated sCO_2 is further heated in tower receiver to desired temperature. Obviously, the outlet temperature of the preheater, namely sCO_2 receiver inlet temperature, varies with solar incident irradiation. Once the required sCO2 receiver inlet temperature is higher than the temperature of the MS at low solar irradiation condition (called critical solar irradiation), the systems cannot operate at full-load condition, the cascade system is closed and the operation strategy of the system is shifted to thermal energy storage mode, meanwhile the bottom steam Rankine cycle can choose whether to work or stop according to grid load using MS as the heat source. Thus the operation mode of the cascade system can be classified into four modes, namely (A) thermal storage mode (B) full-load operation without thermal storage (C) full-load operation with thermal storage and (D) bottom partial-load mode using MS as the heat source. The calculation flow charts for different operation Modes are presented in **Appendix** .

To exhibit flexible adjustment of the cascade system, the critical parameters of the cascade systems, including energy to TES system, sCO_2 inlet temperature, and electricity production, are analyzed when solar irradiation varies from 200 W/m^2 to 900 W/m^2 with the receiver outlet temperature of 800℃ and pressure of 35MPa, as shown in **Figure 14.** In order to simplify the analysis process of the influence of the solar irradiation on system operation strategy, the variations of the solar position and solar concentration distribution of the tower receiver are assumed as identical under different incident solar irradiation. The power capacities of the bottom steam cycle using exhausted sCO_2 and MS as the heat sources are regarded as the same. The powers of the cascade system and the bottom steam cycle are 18.6 MW and 9.2 MW. When the solar irradiation is below 315W/m^2,the required sCO_2 inlet temperature of the receiver is higher than the temperature of the MS, thus the system shifts to **Mode A**; while solar irradiation is between 315 W/m^2 and 500W/m^2, the system can operate at **Mode B** using stored hot MS for preheating sCO_2 and the preheating temperature (required sCO_2 inlet temperature of the receiver) decreases with the increase of the solar irradiation; when solar irradiation is higher than 500W/m^2, the system operates at **Mode C**. The cascade presents stable electricity output and the thermal energy to thermal storage system increases with the increase of the solar irradiation. In conclusion, the cascade system can still work at partial-load using MS as the heat source and keep considerable electricity outputs (about 50% power of the full-load operation) at low solar irradiation (<315W/m^2) or no sun periods. The mass flow rate of the MS is also shown in **Figure 15.** Furthermore, the operation **Mode B** and **C** also can convert to **Mode A** according to electricity grid load. In brief, the cascade system overcome the shortcoming of the simple sCO_2

systems, the thermal energy storage subsystem is combined with a high temperature sCO_2 cycle and operation stability is improved by using thermal energy storage systems. Thus, the cascade system is a promising solar power system to achieve a higher efficiency with stable electricity output and cost-effective thermal energy storage.

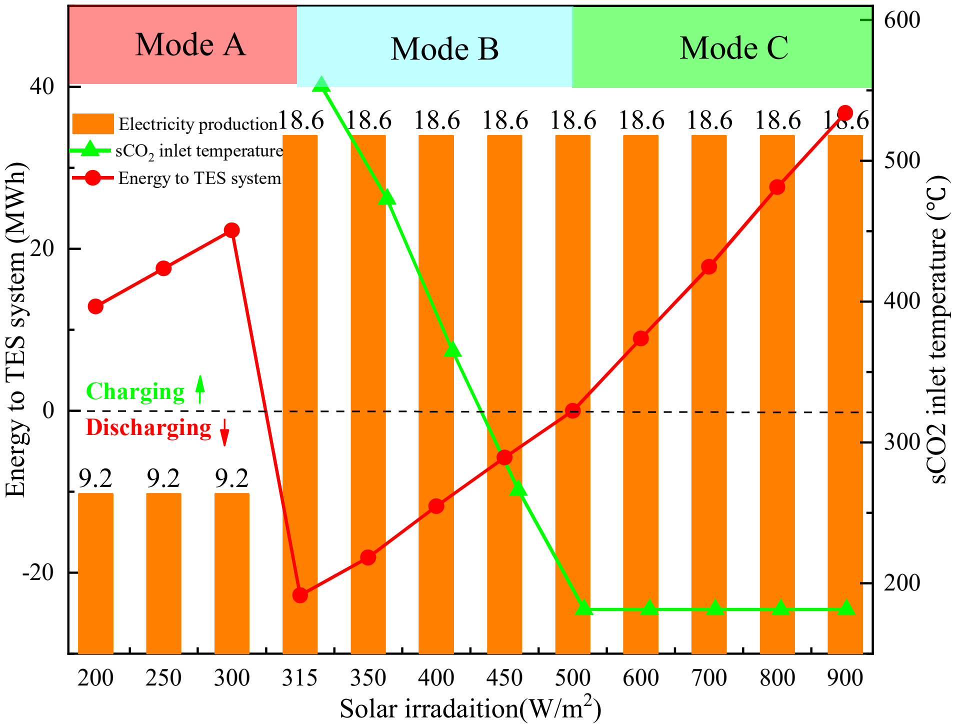

Figure 14 Operation mode of the cascade system

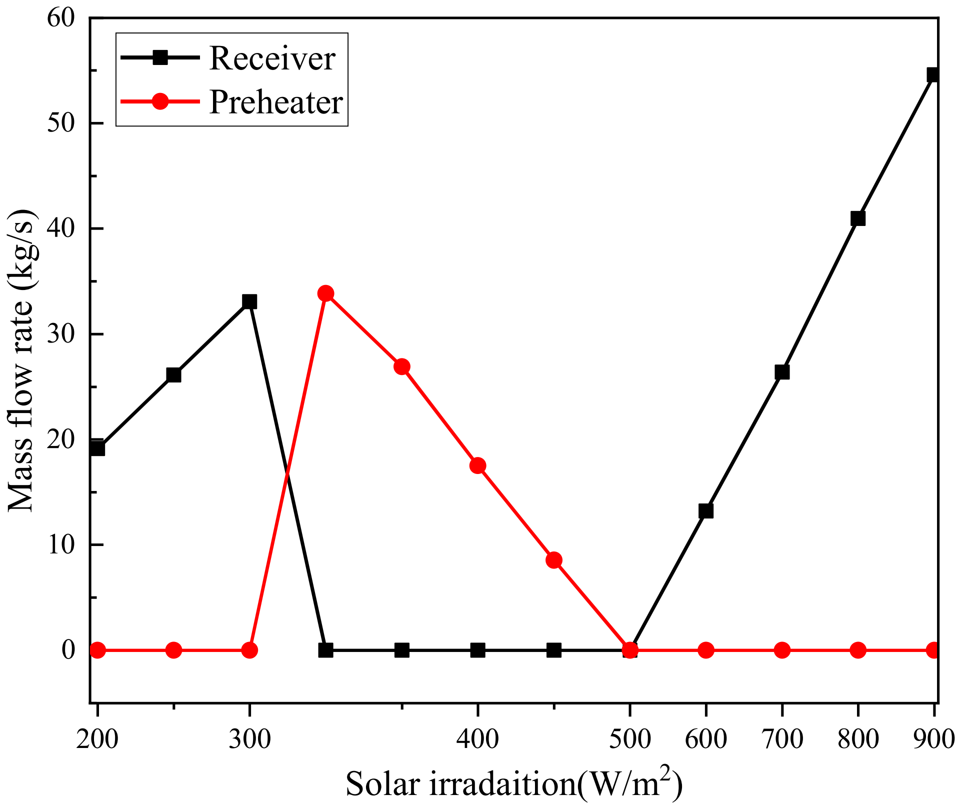

Figure 15 Mass flow rate in receiver and preheater

In **Mode A**, the HTF of the receiver is MS, the MS flow rate increases with the solar incident irradiation. While the HTF of the receiver in **Mode B** is sCO_2, the sCO_2 is firstly preheated in a preheater by the MS. The MS flow rate in preheater decreases with solar irradiation. There is a more complex HTF flow adjustment in **Mode C**. The two different HTFs, MS and sCO2, are adopted in the receiver. To maintain the stable operation of the power block, the mass flow of the sCO_2 is constant under fluctuant solar irradiation by adjusting the length of the sCO_2 solar receiver tube loop and corresponding length of the MS loop is also changed, leading to higher MS flow rate at higher solar irradiation in **Mode C** operation. Based on above analysis, it can be observed that the solar receiver length is assumed variable for different HTF under off-design condition with a constant total length of the receiver tube. In this study, the authors focus on the feasibility investigation and performance superiority of the novel solar tower system using cascade cycle. The detailed design of the solar tower receiver is not discussed. The development of a flexible receiver that can adjust collecting length under different solar irradiation will be focused on in future work.

5. Conclusions

A novel solar power system integrating with supercritical carbon dioxide Brayton-steam Rankine power cycle is proposed to pave a path toward large scale utilization of the supercritical carbon dioxide solar power system. The comprehensive system model is developed to evaluate system performance. The energy and exergy analysis of systems with different configurations are performed. Based on the analysis results, the following conclusions are summarized:

1. The cascade systems have a the lower receiver inlet temperature, wider temperature difference across the receiver, higher specific work of the TES system and lower mass flow rate of the working fluid. The solar-thermal conversion efficiency of the receiver is improved significantly by cascade sCO_2-SR systems. The heat gain of the tower receiver of the cascade system is 53.4 MWh, which is about 7.1 MWh more than that of the simple system for a 10MW solar tower power plant at design point.

2. Solar field optical loss and photo-thermal conversion of the tower receiver are the two biggest exergy losses of the systems. The cooler and supercritical carbon dioxide heat exchanger exergy losses are decreased significantly by the cascade systems.

3. The electricity productions show that cascade system is a promising option for central solar tower systems due to higher optimal operating temperature and efficiency compared to simple supercritical carbon dioxide systems. The electricity productions of simple and cascade systems are 25.2 MWh and 27.6 MWh at 900℃and 35MPa with solar irradiation of 700W/m^2. The electricity production of the cascade system is improved by 9.5%. The cascade system also shows slighter performance

attenuation at off-optimal operation condition.

4. The cascade solar tower system possesses a more flexible operation strategy. The MS is employed as thermal storage medium for achieving continuous and stable operation at the fluctuating condition. The thermal storage issue of the supercritical carbon dioxide systems in the solar thermal power application is solved.

Acknowledgements

This study was sponsored by the National Key R&D of China (2018YFB1900602), National Science Foundation of China (51776193, 51761145109) and the Fundamental Research Funds for the Central Universities (WK6030000133).

Appendix

In this study, the performance of the power plants that possess three different boundary conditions that correspond to different systems operation strategy should be investigated. Firstly, the mass flow calculation of the HTF is presented in **Figure A1** at the given inlet temperature, outlet temperature and solar receiver loop length. Secondly, the preheating temperature calculation of the sCO_2 in **Mode B** operation are presented in **Figure A2** at the given mass flow rate, loop length and outlet temperature. Finally, the length of the sCO_2 loop is variable in **Mode C**, the length calculation of the sCO_2 loop in **Mode C** operation is presented in **Figure A3** at the given mass flow rate, inlet and outlet temperature. Thus, the extra length of the receiver tube is set as MS loop and the flow rate of the MS can be calculated as **Figure A1**. The calculation procedure of the above three different boundary condition is explained one by one as follows:

A.1 Mass flow calculation of the HTF

(1) Initial fixed values, including solar flux distribution of the receiver, dimension parameter of the

receiver and absorber tube, are input;

(2) Initial values of the mass flow *m*, inlet temperature T_{in}, and outlet temperature T_{out} are input;

(3) Initial values of the outer surface of the absorber temperature $T_{\mathrm{abs,o}}$ are input;

(4) With T_{absi}, *m*, Q_{abs}, Q_{conv}, Q_{cond}, and Q_{loss} are calculated by Eqs. (4–8) and (20);

(5) With the calculated Q_{conv}, Q_{cond}, and Q_{loss}, the new value of the outer surface of receiver tube is calculated;

(6) Go back to Step (4). The calculation is carried out with the same process until the absolute temperature difference of $T_{\mathrm{abs,o}}$ and T_{abs} is below 0.1°C;

(7) Go back to Step (3). The calculation is carried out with the same process until a whole loop *L* of receiver is evaluated;

(8) Go back to Step (3). The new value of mass flow rate is calculated. Calculation is carried out with same process until the absolute difference of T_{outi} and T_{out} is below 0.1°C;

(9) The simulation results are output.

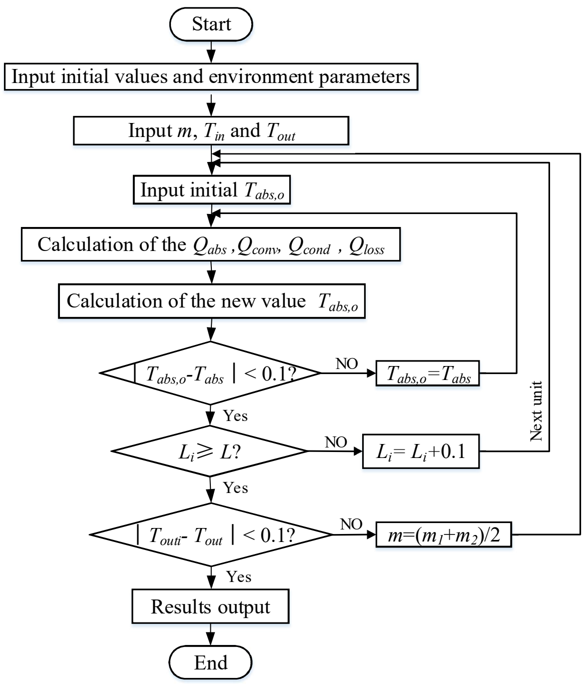

Figure A1 Flow chart of the mass flow rate calculation

A.2 sCO2 preheating temperature calculation

(1) Same as **Appendix A.1**

(2) Same as **Appendix A.1**

(3) Same as **Appendix A.1**

(4) Same as **Appendix A.1**

(5) Same as **Appendix A.1**

(6) Same as **Appendix A.1**

(7) Same as **Appendix A.1**

(8) Go back to Step (3). The new value of inlet temperature is calculated. Calculation is carried out with same process until the absolute difference of T_{outi} and T_{out} is below 0.1°C;

(9) The simulation results are output.

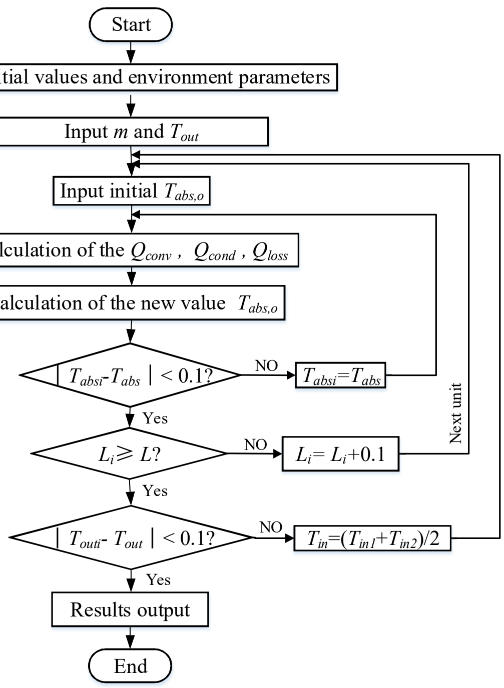

Figure A2 Flow chart of the sCO2 preheating temperature calculation

A.3 sCO2 loop length *L* calculation

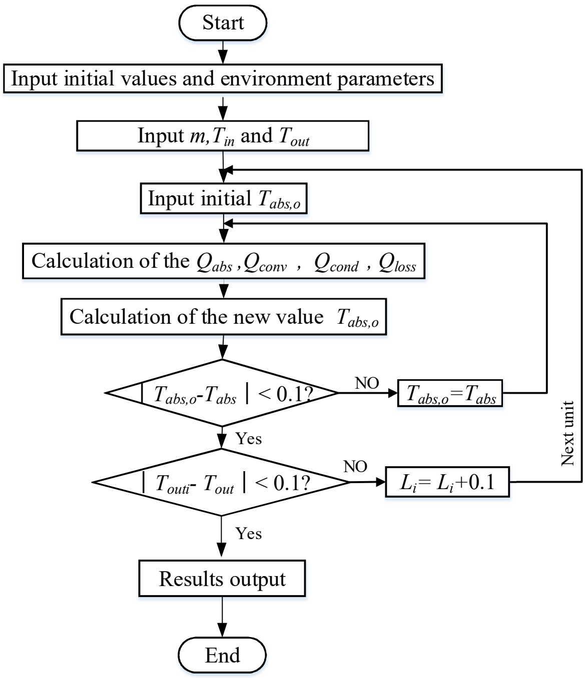

Figure A3 Flow chart of the sCO2 loop length calculation

(1) Same as **Appendix A.1**

(2) Same as **Appendix A.1**

(3) Same as **Appendix A.1**

(4) Same as **Appendix A.1**

(5) Same as **Appendix A.1**

(6) Same as **Appendix A.1**

(7) Go back to Step (3). The calculation is carried out with same process until the absolute difference of T_{outi} and T_{out} is below 0.1°C;

(8) The simulation results are output.

References

[1] Ju, X., Xu, C., Hu, Y., et al. A review on the development of photovoltaic/concentrated solar power (PV-CSP) hybrid systems. Solar Energy Materials & Solar Cells, 2017, 161: 305-27

[2] Kincaid, N., Mungas, G., Kramer, N., et al. An optical performance comparison of three concentrating solar power collector designs in linear Fresnel, parabolic trough, and central receiver. Applied Energy, 2018, 231: 1109-21

[3] Bai, Z., Sun, J., Liu, Q. Comprehensive assessment of line‐/point‐focus combined scheme for concentrating solar power system. International Journal of Energy Research , 2018, 42: 1983-98

[4] Dowling, A. W., Zheng, T., Zavala, V. M. J. R., et al. Economic assessment of concentrated solar power technologies: a review. Renewable and Sustainable Energy Reviews, 2017, 72: 1019-32

[5] Stein, W., Buck, R. Advanced power cycles for concentrated solar power. Solar Energy, 2017, 152: 91-105

[6] Jiang, D., Xu, H., Khan, H. I., et al. Transport of corrosion products in the steam-water cycle of supercritical power plant. Applied Thermal Engineering, 2017, 113: 1164-9

[7] Sun, E., Xu, J., Hu, H., et al. Overlap energy utilization reaches maximum efficiency for S-CO2 coal fired power plant: A new principle. Energy Conversion and Management, 2019, 195: 99-113

[8] Fleming, D., Holschuh, T., Conboy, T., et al. Scaling Considerations for a Multi-Megawatt Class Supercritical CO2 Brayton Cycle and Path Forward for Commercialization. Conference Scaling Considerations for a Multi-Megawatt Class Supercritical CO2 Brayton Cycle and Path Forward for Commercialization, 2012, 44717: 953-60.

[9] Luu, M. T., Milani, D., McNaughton, R., et al. Analysis for flexible operation of supercritical CO2 Brayton cycle integrated with solar thermal systems. Energy, 2017, 124: 752-71

[10] Sulzer G. Verfahren zur Erzeugung von Arbeit aus Warme. Swiss Patent. 1950;269599.

[11] Feher, E. G. The supercritical thermodynamic power cycle. Energy conversion, 1968,8(2): 85-90.

[12] Dostal, V., Driscoll, M. J., Hejzlar, P. A supercritical carbon dioxide cycle for next generation nuclear reactors. Massachusetts: Massachusetts Institute of Technology, Department of Nuclear Engineering, 2004.

[13] Cheng, W.-L., Huang, W.-X., Nian, Y.-L. Global parameter optimization and criterion formula of supercritical carbon dioxide Brayton cycle with recompression. Energy Conversion and Management, 2017, 150: 669-77

[14] Moisseytsev, A., Sienicki, J. Performance improvement options for the supercritical carbon dioxide brayton cycle. Argonne: Argonne National Lab.(ANL), Argonne, IL (United States); 2008.

[15] Sun, E., Xu, J., Li, M., et al. Connected-top-bottom-cycle to cascade utilize flue gas heat for supercritical carbon dioxide coal fired power plant. Energy Conversion and Management, 2018, 172: 138-54

[16] Xu, J., Sun, E., Li, M., et al. Key issues and solution strategies for supercritical carbon dioxide coal fired power plant. Energy, 2018, 157: 227-46

[17] Wang, K., He, Y.-L., Zhu, H.-H. J. A. e. Integration between supercritical CO2 Brayton cycles and molten salt solar power towers: A review and a comprehensive comparison of different cycle layouts. Applied Energy, 2017, 195: 819-36

[18] Qiu, Y., Li, M. J., He, Y. L., et al. Thermal performance analysis of a parabolic trough solar collector using supercritical CO2 as heat transfer fluid under non-uniform solar flux. Applied Thermal Engineering, 2016: 1255-65

[19] Wang, K., He, Y.-L. Thermodynamic analysis and optimization of a molten salt solar power tower integrated with a recompression supercritical CO 2 Brayton cycle based on integrated modeling. Energy Conversion and Management, 2017, 135: 336-50

[20] Reyes-Belmonte, M., Sebastián, A., Romero, M., et al. Optimization of a recompression supercritical carbon dioxide cycle for an innovative central receiver solar power plant. Energy, 2016, 112: 17-27

[21] Khatoon, S., Kim, M. H. Performance analysis of carbon dioxide based combined power cycle for concentrating solar power. Energy Conversion & Management, 2020, 205: 112416

[22] Zhu, H. H., Wang, K., He, Y. L. Thermodynamic analysis and comparison for different direct-heated supercritical CO 2 Brayton cycles integrated into a solar thermal power tower system. Energy, 2017, 140: 144-57

[23] Padilla, R. V., Soo Too, Y. C., Benito, R., et al. Exergetic analysis of supercritical CO 2 Brayton cycles integrated with solar central receivers. Applied Energy, 2015, 148: 348-65

[24] Turchi, C. S., Vidal, J., Bauer, M. J. S. E. Molten salt power towers operating at 600–650 C: Salt selection and cost benefits. Solar Energy, 2018, 164: 38-46

[25] He, Y.-L., Qiu, Y., Wang, K., et al. Perspective of concentrating solar power. Energy, 2020: 117373

[26] FluxSPT software. ISE Research Group. http://ise.uc3m.es/research/solar-energy/heliostat-field/

[27] Sánchez-González, A., Rodríguez-Sánchez, M. R., Santana, D. Aiming factor to flatten the flux distribution on cylindrical receivers. Energy, 2018, 153: 113-25

[28] Bergman, T. L., Lavine, A. S., Incropera, F. P., et al. Fundamentals of heat and mass transfer. John Wiley & Sons Hoboken, NJ; 2011.

[29] Modest, M. F. Radiative heat transfer. Academic press, 20130.

[30] Siebers, D L, and Kraabel, J S. Estimating convective energy losses from solar central receivers. United States: N. p., 1984.

[31] Lemmon, E W, Huber, M L, McLinden, M O. NIST Standard Reference Database 23: reference fluid thermodynamic and transport properties - REFPROP, version 9.1, Standard Reference Data Program, National Institute of Standards and Technology. Nist Nsrds, 2010.

[32] Giwa, A., Hasan, S. W. J. D. Novel thermosiphon-powered reverse osmosis: Techno-economic model for renewable energy and fresh water recovery. Desalination 2018; 435: 152-60.

[33] Bejan, A. Advanced engineering thermodynamics: John Wiley & Sons, 2016.

[34] Kulhánek, M., Dostal, V. Thermodynamic analysis and comparison of supercritical carbon dioxide cycles. Conference Thermodynamic analysis and comparison of supercritical carbon dioxide cycles, 2011: 24-5.

[35] Turchi, C. S., Ma, Z., Neises, T. W., et al. Thermodynamic study of advanced supercritical carbon dioxide power cycles for concentrating solar power systems. Journal of Solar Energy Engineering, 2013, 135: 041007

[36] Xu, L., Wesley, S., Jin-Soo, K., et al. Transient numerical model for the thermal performance of the solar receiver. Applied Thermal Engineering, 2018,141: 1035-1047.

***Credit Author Statement**

Honglun Yang: Conceptualization, Data curation, Formal analysis, Investigation, Methodology; Software; Validation; Visualization; Writing - original draft; Writing - review & editing; **Jing Li:** Conceptualization, Data curation, Formal analysis, Investigation, Methodology; Software; Writing - review & editing; **Qiliang Wang:** Data curation, Validation; **Lijun Wu**: Writing - review &editing; **María Reyes Rodríguez-Sanchez**: Formal analysis, Data curation, Validation; **Domingo Santana:** Methodology; Project administration; Resources; Supervision; **Gang Pei**: Conceptualization, Funding acquisition; Methodology; Project administration; Resources; Supervision; Roles/Writing - original draft; Writing - review & editing.

***Declaration of Interest Statement**

Declaration of interests

☒ The authors declare that they have no known competing financial interests or personal relationships that could have appeared to influence the work reported in this paper.

☐The authors declare the following financial interests/personal relationships which may be considered as potential competing interests: